Polymer Chemistry

PAPER

View Article Online
View Journal | View Issue

Cite this: *Polym. Chem.*, 2015, **6**, 6219

Dithieno[3,2-*b*:2′,3′-*d*]silole-based low band gap polymers: the effect of fluorine and side chain substituents on photovoltaic performance†

Chuantao Gu,[a,c] Qianqian Zhu,[b] Xichang Bao,[a] Shuguang Wen,[a] Meng Qiu,[a] Liangliang Han,[a] Wei Huang,[a] Dangqiang Zhu[a,c] and Renqiang Yang*[a,d]

Received 4th June 2015,
Accepted 13th July 2015

DOI: 10.1039/c5py00849b

www.rsc.org/polymers

Three alkyl-thiophene π-bridged polymers, PDTS-*h*DTFBT (**P-*h*F**), PDTS-*h*DTDFBT (**P-*h*DF**) and PDTS-*eh*DTDFBT (**P-*eh*DF**), with different number of F atoms and side chain substituents are synthesized through a palladium catalyzed Stille coupling reaction. **P-*h*F**, **P-*h*DF** and **P-*eh*DF** show a narrow band gap of 1.56, 1.56 and 1.60 eV with deep lying highest-occupied molecular orbital (HOMO) energy levels of −5.17, −5.21 and −5.35 eV, respectively. The optimized **P-*h*DF**-based photovoltaic device exhibits an open circuit voltage of 0.593 V, a short-circuit current density of 15.98 mA cm^{-2}, a fill factor of 64.8% and a high energy conversion efficiency of 6.14%, which is partially ascribed to the deep HOMO energy level and good coplanarity. The performance is among the highest reported ones in devices based on polymers with dithieno[3,2-*b*:2′,3′-*d*]silole (DTS) as the electron-rich unit and 2,1,3-benzothiadiazole (BT) derivatives as the electron-deficient unit.

Introduction

Harvesting energy directly from sunlight using photovoltaic technology is considered as one of the most important ways to address growing global energy needs using a renewable resource.[1] Polymer solar cells (PSCs) have attracted considerable interest from both the academic and industrial communities over the past decade due to advantages such as easy processability over a large-area size *via* printing or roll-to-roll technologies, low-cost manufacturing, and compatibility with flexible substrates.[1–7] Three key parameters that determine the power conversion efficiency (PCE) of a solar cell are open-circuit voltage (V_{OC}), short-circuit current density (J_{SC}) and fill factor (FF). PCE is equal to the product of these three parameters divided by the input power.[2,8,9] Despite the many advantages of PSCs, a low PCE is still a major impediment to real commercialization.[10,11] Although remarkable progress has been achieved by optimization of the device architectures and developing ideal photovoltaic polymers over the past decade, which led to a higher than 10% PCE,[12–14] further improvements are needed for mass production and practical applications. The most successful strategy to improve the PCE is to develop new low band gap donor materials[15,16] to enlarge overlap with the solar spectrum in the infrared region and ensure efficient harvesting of solar photons, which could improve J_{SC}.

A variety of low band gap conjugated polymers have been designed and synthesized by scientists during the past few decades. One representative polymer is poly[4,4-bis(2-ethylhexyl)-4*H*-cyclopenta[2,1-*b*:3,4-*b*′]dithiophene-2,6-diyl-*alt*-2,1,3-benzothiadiazole-4,7-diyl] (PCPDTBT). The PSCs based on PCPDTBT:[6,6]-phenyl-C71-butyric acid methyl ester ($PC_{71}BM$) showed a moderate PCE of 5.5%,[17] which is mainly limited by the low FF and V_{OC}. There are two main strategies to improve the photovoltaic performance of PCPDTBT. The first one is the introduction of strong electron-withdrawing fluorine atom(s) to the electron-deficient unit of the polymer. F-containing PCPDTBTs (PCPDTFBT and PCPDTDFBT) have been reported by several groups.[18–22] Their encouraging results showed that the highest-occupied molecular orbital (HOMO) energy levels could be lowered by introducing fluorine atom(s) to the electron-deficient unit, as a result, V_{OC} was increased. However, the solubility has been reduced[18,20,21] due to the enhanced F–H, F–F interactions and strong stacking[23] of polymers; especially for the PCPDTDFBT, the PCE decreased to 3.37%.[21]

[a]*CAS Key Laboratory of Bio-based Materials, Qingdao Institute of Bioenergy and Bioprocess Technology, Chinese Academy of Sciences, Qingdao 266101, China. E-mail: yangrq@qibebt.ac.cn; Fax: +86-532-80662778; Tel: +86-532-80662700*
[b]*College of Materials Science and Engineering, Qingdao University of Science and Technology, Qingdao 266042, China*
[c]*University of Chinese Academy of Sciences, Beijing 100049, China*
[d]*State Key Laboratory of Luminescent Materials and Devices, South China University of Technology, Guangzhou 510641, China*

†Electronic supplementary information (ESI) available: X-ray diffraction, TGA and DSC thermograms, computational study, detailed device parameters of PSCs, and hole mobility. See DOI: 10.1039/c5py00849b

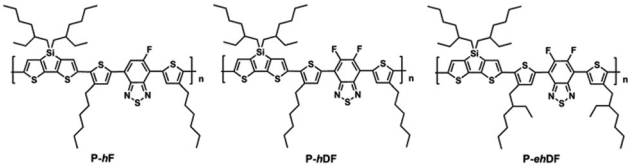

Fig. 1 Chemical structures of P-*h*F, P-*h*DF and P-*eh*DF.

4-Hexylthiophene had been introduced to PCPDTDFBT as a π-bridge to improve the solubility in our previous work, and the PCE increased from 3.37% to 5.85%.[24] The other method is the replacement of the carbon atom at the 4-position of cyclopenta[2,1-*b*:3,4-*b*′]dithiophene by a silicon atom. The properties of Si-PCPDTBT, named poly[(4,4′-bis(2-ethylhexyl)-dithieno[3,2-*b*:2′,3′-*d*]silole)-2,6-diyl-*alt*-2,1,3-benzothiadiazole-4,7-diyl] (PDTSBT), have been studied by several groups,[25–28] their results showed that the silicon atom fusion enhances solid-state ordering compared to the carbon-fused analogue, resulting in improved charge transport, which is favorable to obtain a higher J_{SC} value.[29] Y. Yang indicated that the long Si–C bonds displaced the solubilizing side chains further from the thiophene rings, allowing a stronger π-stacking interaction to occur, which was the possible reason for the improved charge transport.[28] However, the solubility of the strong stacking Si-bridged polymers decreased in common organic solvents.[27]

In this work, in order to obtain a deeper HOMO and a higher J_{SC}, the two strategies were combined, an F atom was introduced to the electron-deficient unit and the carbon bridge was substituted by a silicon atom simultaneously. 4-Hexylthiophene is employed as a π-bridge to improve the solubility similar to our previous work.[24] The structures of the resulting polymers, PDTS-*h*DTFBT (here referred to as **P-*h*F**) and PDTS-*h*DTFDBT (here referred to as **P-*h*DF**), are shown in Fig. 1. Previous studies have demonstrated that conformational twisting of the main chain of a polymer is an effective method to lower the HOMO energy level.[30–32] Thus, to further improve the V_{OC}, the steric group 2-ethylhexyl was introduced to the thiophene π-bridge, the third polymer was named PDTS-*eh*DTDFBT (here referred to as **P-*eh*DF**). The thermal stability, and photophysical, electrochemical and photovoltaic properties of the polymers were carefully investigated. The **P-*h*DF**/$PC_{71}BM$ based PSC gave a promising PCE of 6.14% with a J_{SC} of 15.98 mA cm^{-2}, a V_{OC} of 0.593 V and an FF of 64.8%. The **P-*eh*DF**/$PC_{71}BM$ based PSC showed a higher V_{OC} of 0.805 V as expected.

Results and discussion

Synthesis and characterization

Three polymers were synthesized in good yield (76–83%) by Stille coupling polymerization, using a $Pd_2(dba)_3$/P(*o*-tol)$_3$ catalytic system. The polymers were purified by Soxhlet extraction with methanol, hexane, and $CHCl_3$ in succession. $CHCl_3$ fractions were collected, concentrated, reprecipitated in methanol, and dried under vacuum overnight to offer the target polymers. All polymers show excellent solubility in common organic solvents, such as chloroform, chlorobenzene (CB), and dichlorobenzene (DCB). The polymers can even partially dissolve in dichloromethane. The good solubility could be attributed to the alkylthiophene π-bridge. The molecular weight and polydispersity index (PDI) were determined by gel permeation chromatography (GPC) with calibration against polystyrene standards and tetrahydrofuran (THF) as the eluent. The number average molecular weights (M_n) of **P-*h*F**, **P-*h*DF** and **P-*eh*DF** were found to be 15.4, 16.2 and 12.8 kg mol^{-1}, with PDIs of 1.86, 1.74 and 2.19, respectively. The crystallinity of the polymer films was investigated using X-ray diffraction (XRD) spectra (Fig. S1†). There are no peaks observed for the polymers, indicating their amorphous nature.[33] The thermal stability of the polymers was explored by thermogravimetric analysis (TGA) and differential scanning calorimetry (DSC), as shown in Fig. S2.† The three polymers have good thermal stability with onset decomposition temperatures (T_d) corresponding to a 5% weight loss at 431 °C, 424 °C and 432 °C, respectively. DSC plots reveal that there is no obvious glass transition for the polymers before 420 °C. Obviously, the thermal stability of the polymers is adequate for their applications in PSCs devices.

Computational study

The conformational analysis as well as calculations of energies and distributions of the frontier molecular orbitals of these polymers were performed by density functional theory (DFT) using the Gaussian 09 program at the B3LYP/6-31G(d,p) level in the gas phase.[34] The optimized molecular geometries were confirmed to be minimum-energy conformations since there were no imaginary frequencies by vibrational calculation at the same level. In this work, one repeat unit was chosen, and alkyl chains were simplified to reduce the calculation time (2-ethylhexyl on dithieno[3,2-*b*:2′,3′-*d*]silole (DTS) was simplified into methyl, hexyl on the thiophene π-bridge of **P-*h*F** and **P-*h*DF** was simplified into propyl, and 2-ethylhexyl on the thiophene π-bridge of **P-*eh*DF** was simplified into isobutyl). The energies and distributions of the frontier molecular orbitals of the polymers are shown in Fig. S3.† Fig. 2 presents the energy minimized conformational structures. The fluorine substituent has a great influence on inter- or intramolecular interactions.[35] The noncovalent attractive interaction was demonstrated to be

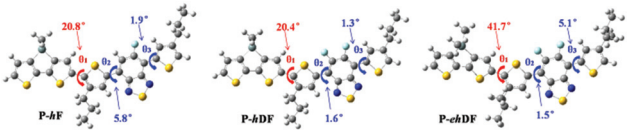

Fig. 2 Minimum energy conformations of the polymers. Color code: gray (C), white (H), blue (N), yellow (S), cyan (Si) and light blue (F).

effective for minimizing the torsional angles within the polymer backbones.[23,35] Compared with **P-*h*F**, the introduction of the second F atom in **P-*h*DF** lowers the HOMO energy level (−4.889 eV) and decreases the dihedral angle between 2,1,3-benzothiadiazole (BT) and thiophene (θ_2, θ_3) due to the enhanced F–H, F–F interactions and strong stacking.[23,35] The second F atom has little effect on the dihedral angle between dithieno[3,2-*b*:2′,3′-*d*]silole (DTS) and thiophene (θ_1). In other words, the coplanarity of **P-*h*DF** was better than that of **P-*h*F**, and a higher J_{SC} of the **P-*h*DF**-based device could be expected.[1,35–39] The introduction of 2-ethylhexyl in **P-*eh*DF** further lowers the HOMO energy level to −4.985 eV and increases the dihedral angle θ_1 to 41.7° due to the large steric hindrance. Therefore, a higher V_{OC} of **P-*eh*DF**-based device can be expected.

Optical properties

The ultraviolet-visible (UV-vis) absorption spectra of the polymers in dilute chloroform solution and thin films spin-coated on a glass substrate are shown in Fig. 3. The detailed absorption data are summarized in Table 1. These polymers show similar absorption bands in solution with major absorption peaks at 596, 582 and 569 nm for **P-*h*F**, **P-*h*DF** and **P-*eh*DF**, respectively. This characteristic peak can be attributed to the intramolecular charge transfer (ICT) between donor units and acceptor units.[18] The other absorption band near 430 nm was due to the π–π* transition.[40] In the solid state, the main absorption peaks become broader and red shift toward a longer wavelength with maximum absorption peaks at 655, 645 and 621 nm for **P-*h*F**, **P-*h*DF** and **P-*eh*DF**, respectively. This behavior is ascribed to the enhanced intermolecular interactions between the polymer main chains and the planarization effect of the π-conjugated polymer backbone.[24] The more red shifts from solution to solid film means a better coplanar structure and stronger interchain π–π stacking in the solid state,[28,41] which is favorable to obtain a higher J_{SC}.[35–39] The red shifts of **P-*h*F**, **P-*h*DF** and **P-*eh*DF** were 59, 63 and 52 nm, respectively. It means that **P-*h*F** and **P-*h*DF** showed a bigger red shift than that of **P-*eh*DF**, which may be ascribed to the larger steric hindrance of a 2-ethylhexyl side chain on the π-bridge of **P-*eh*DF** thus distorting the backbone (Fig. 2). The optical band gap (E_g^{opt}) of **P-*h*F**, **P-*h*DF** and **P-*eh*DF** can be calculated to be 1.56, 1.56 and 1.63 eV, respectively, from their onset absorption as thin films. It has been proven that attaching a fluorine atom to the electron deficient subunits of low band gap polymers could simultaneously lower the HOMO and lowest unoccupied molecular orbital (LUMO) level energies, while having no or only a minor effect on the E_g^{opt}.[20,42,43] The same E_g^{opt} of **P-*h*F** and **P-*h*DF** is in agreement with previously reported results. The larger E_g^{opt} of **P-*eh*DF** may be ascribed to the tortuous polymer backbone which was caused by the stronger steric hindrance[31,32] of the 2-ethylhexyl side chain on the π-bridge.

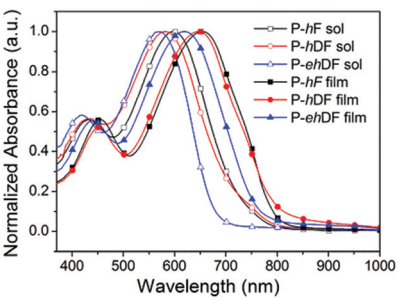

Fig. 3 UV-vis absorption spectra of **P-*h*F**, **P-*h*DF** and **P-*eh*DF** in chloroform solutions and as thin films.

Electrochemical properties

Cyclic voltammetry (CV) measurement was performed to investigate the electrochemical properties of the polymers. The saturated calomel reference electrode (SCE) was calibrated against the Fc/Fc^+ system to be 4.41 eV in this work. As shown in Fig. 4a, all polymers show reversible oxidation behaviors. The onsets of oxidation potentials (E_{on}^{ox}) of **P-*h*F**, **P-*h*DF** and **P-*eh*DF** were observed at 0.76, 0.80 and 0.94 V *vs.* SCE, corresponding to the HOMO levels at −5.17, −5.21 and −5.35 eV, respectively. The onsets of reduction potentials (E_{on}^{red}) of **P-*h*F**, **P-*h*DF** and **P-*eh*DF** were observed at −0.70, −0.67 and −0.60 V *vs.* SCE, corresponding to the LUMO levels at −3.71, −3.74 and −3.80 eV, respectively. Relevant data are summarized in Table 1. The HOMO of **P-*h*DF** is slightly lower than that of **P-*h*F**, which is caused by the second electron-withdrawing F atom. Interestingly, **P-*eh*DF** exhibited a more deeper HOMO of −5.35 eV, which can be ascribed to the synergistic effect of the two F atoms and the distorted polymer backbone caused by the steric hindrance effect of the 2-ethylhexyl side chain on the π-bridge,[31,32] and the result was consistent with the calculations. Therefore, a higher V_{OC} in **P-*eh*DF**-based PSCs can be expected, since V_{OC} is proportional to the offset between the

Table 1 Optical, electrochemical and thermal properties of **P-*h*F**, **P-*h*DF** and **P-*eh*DF**

	Solution[a]		Thin film					
Polymer	λ_{max} (nm)	λ_{onset} (nm)	λ_{max} (nm)	λ_{onset} (nm)	E_g^{opt} [b] (eV)	E_{on}^{ox}/HOMO[c] (V/eV)	E_{on}^{red}/LUMO[d] (V/eV)	T_d (°C)
P-*h*F	596	733	655	796	1.56	0.76/−5.17	−0.70/−3.71	431
P-*h*DF	582	718	645	796	1.56	0.80/−5.21	−0.67/−3.74	424
P-*eh*DF	569	676	621	760	1.63	0.94/−5.35	−0.61/−3.80	432

[a] Absorption data were collected in $CHCl_3$ solution. [b] Data obtained by the absorption edge of the thin film, $E_g^{opt} = 1240/\lambda_{onset}$. [c] HOMO = $-(E_{on}^{ox} + 4.41)$ eV, where E_{on}^{ox} is the onset oxidation potential. [d] LUMO = $-(E_{on}^{red} + 4.41)$ eV, where E_{on}^{red} is the onset reduction potential.

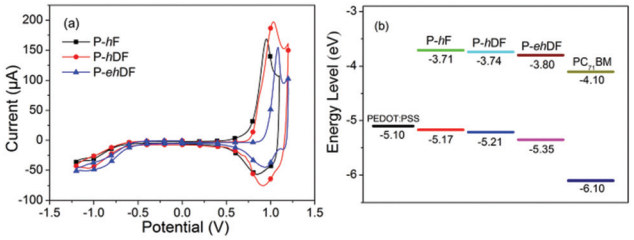

Fig. 4 Cyclic voltammograms (a) and the energy level diagram (b) of P-*h*F, P-*h*DF and P-*eh*DF.

Table 2 PSCs performance with device configuration ITO/PEDOT/polymer:$PC_{71}BM$/Ca/Al

Active layer	Ratio	DIO (%)	V_{OC} (V)	J_{SC} (mA cm^{-2})	FF (%)	PCE (%)
P-*h*F : $PC_{71}BM$	1 : 1	0	0.620	14.04	53.5	4.66
P-*h*F : $PC_{71}BM$	1 : 1	0.5	0.553	15.51	58.8	5.04
P-*h*DF : $PC_{71}BM$	1 : 1	0	0.683	10.90	64.0	4.76
P-*h*DF : $PC_{71}BM$	1 : 1	1	0.593	15.98	64.8	6.14
P-*eh*DF : $PC_{71}BM$	1 : 2	0	0.805	8.01	62.6	4.03
P-*eh*DF : $PC_{71}BM$	1 : 2	2	0.749	5.11	52.4	2.01

HOMO of the polymeric donor and the LUMO of the fullerene acceptor.[43] In order to make a clear comparison, the electronic energy level diagram of these polymers and $PC_{71}BM$ is shown in Fig. 4b. The LUMO differences between the polymers and $PC_{71}BM$ are 0.39, 0.36 and 0.30 eV, respectively, and they are large enough to overcome the exciton binding energy and thus guarantee efficient exciton dissociation and transfer.[38,43,44]

Photovoltaic performance

In order to examine the photovoltaic properties of these polymers, the bulk heterojunction PSCs were fabricated with a device structure of ITO/PEDOT:PSS/polmer:$PC_{71}BM$/Ca/Al, and tested under a simulated AM 1.5G illumination of 100 mW cm^{-2}. Several batch devices were prepared to optimize the processing conditions such as the polymer to $PC_{71}BM$ weight ratio and the additive 1,8-diiodooctane (DIO) concentration. The current density *vs.* voltage (*J*–*V*) curves are shown in Fig. 5, and the detailed device parameters are summarized in Tables 2 and S1.† One can observe that the V_{OC} of **P-*h*DF** is higher than that of **P-*h*F**, which could be ascribed to the low lying HOMO of **P-*h*DF** caused by the second F atom. Surprisingly, the V_{OC} of **P-*eh*DF** is more than 0.1 V and higher than that of **P-*h*DF**, resulting from the lower lying HOMO of **P-*eh*DF** due to the two F atoms and twisted polymer backbone caused by the larger steric hindrance[30,31] of the 2-ethylhexyl side chain on the π-bridge. The result is in accordance with the energy level obtained from CV and calculations. The V_{OC} of all polymers were decreased after the addition of DIO, which is consistent with previous reports.[20,45,46] The addition of DIO to the blend solution is found to increase J_{SC} and FF in **P-*h*F** and **P-*h*DF** based devices, however, J_{SC} and FF decreased in **P-*eh*DF** based devices. The J_{SC} of **P-*h*F** and **P-*h*DF** based devices was optimized to 15.51 and 15.98 mA cm^{-2}, which was higher than that of their carbon-analogues (10.88 and 13.58 mA cm^{-2}).[24] This could be attributed to the stronger π-stacking interaction and enhanced solid state ordering compared to the carbon-fused analogue.[27–29] Finally, the highest PCE of 6.14% for **P-*h*DF** is obtained with a V_{OC} of 0.593 V, a J_{SC} of 15.98 mA cm^{-2}, and a FF of 64.8%, when the device was fabricated at a donor–acceptor weight ratio of 1 : 1 in DCB with a total concentration of 24 mg mL^{-1} containing 1% DIO as an additive.

External quantum efficiency (EQE) curves of the devices based on these polymers prepared with the optimal fabrication processes are shown in Fig. 6. It can be seen that the devices exhibit a broad response over the range 320–780 nm. The EQE value between 350 and 700 nm for the **P-*h*DF** device is slightly higher than that of the **P-*h*F** device. Although the **P-*eh*DF** device exhibits a broad response, yet the EQE peak value is only 39%. The integrated J_{SC} from EQE is 15.19, 15.57 and 7.70 mA cm^{-2} for **P-*h*F**, **P-*h*DF** and **P-*eh*DF** based devices, respectively, which are consistent with the measured J_{SC} values. Mobility measurements *via* a space charge limited current (SCLC) method[42,46,47] disclose a hole mobility of 2.02 × 10^{-4} cm^2 V^{-1} s^{-1} for the **P-*h*F** : $PC_{71}BM$ device and 2.53 × 10^{-4} cm^2 V^{-1} s^{-1} for the **P-*h*DF** : $PC_{71}BM$ device (Fig. S4†), both three orders of magnitude higher than that of the **P-*eh*DF** : $PC_{71}BM$ device (4.77 × 10^{-7} cm^2 V^{-1} s^{-1}). The low hole mobility

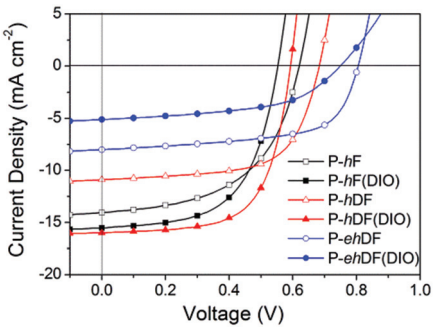

Fig. 5 *J*–*V* curves of polymer/$PC_{71}BM$-based regular single solar cells under AM 1.5 G illumination, 100 mW cm^{-2}.

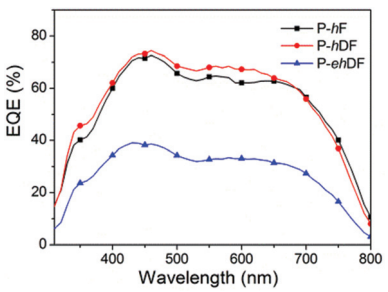

Fig. 6 EQE curves for blends of P-*h*F, P-*h*DF and P-*eh*DF with $PC_{71}BM$ processed from DCB solutions.

may be caused by the increased dihedral angle between the donor unit and the flanking thiophene rings (Fig. 2), which decrease the coplanarity of the backbone.[35,46] The quite low hole mobility could be due to an intrinsic reason that the **P-*eh*DF** : $PC_{71}BM$ device exhibits lower J_{SC}.[36]

Morphology study

To deeply understand the different photovoltaic properties, atom force microscopy (AFM) images of the active layer surface for the best performance device without or with DIO were collected. Fig. 7 shows the height images of **P-*h*F** : $PC_{71}BM$ (1 : 1), **P-*h*DF** : $PC_{71}BM$ (1 : 1) and **P-*eh*DF** : $PC_{71}BM$ (1 : 2) blend films processed without or with the DIO additive, and the corresponding phase images are shown in Fig. 8. The surface of the **P-*h*F** : $PC_{71}BM$ film without DIO was packed with small holes with a root-mean-square (RMS) surface roughness of 0.80 nm (Fig. 7a). When processed with 0.5% DIO (Fig. 7d), the film formed a pin-hole free and a little rough surface topography (RMS = 1.59 nm). The surfaces of the **P-*h*DF** : $PC_{71}BM$ film without (Fig. 7b) or with (Fig. 7e) DIO were both uniform without holes. The RMS was increased from 1.57 nm to 5.41 nm after addition of 1% DIO, indicating appropriately

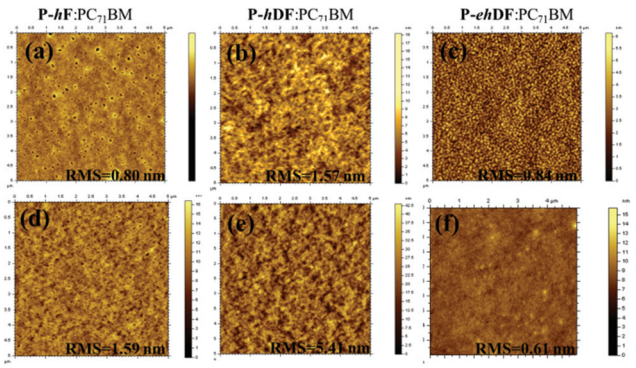

Fig. 7 AFM height images of the active layer containing **P-*h*F** : $PC_{71}BM$ (a, d), **P-*h*DF** : $PC_{71}BM$ (b, e) and **P-*eh*DF** : $PC_{71}BM$ (c, f) without (top) or with (bottom) DIO. The scan size is 5 μm × 5 μm.

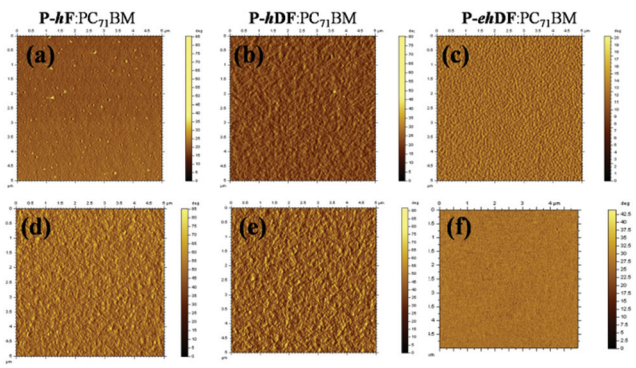

Fig. 8 AFM phase images of the active layer containing **P-*h*F** : $PC_{71}BM$ (a, d), **P-*h*DF** : $PC_{71}BM$ (b, e) and **P-*eh*DF** : $PC_{71}BM$ (c, f) without (top) or with (bottom) DIO. The scan size is 5 μm × 5 μm.

enhanced aggregations (Fig. 8e).[48] Using DIO can usually facilitate obtaining appropriate phase-separated domains. If the phase-separated domains are preferable without DIO in some systems of polymer/$PC_{71}BM$, the additive of DIO would not result in higher PCE.[8,46,49,50] For the **P-*eh*DF** : $PC_{71}BM$ blending film, the addition of 2% DIO resulted in quite a smooth surface topography (RMS = 0.61 nm, Fig. 7f) but without effective phase separation (Fig. 8f), which may be a main reason that **P-*eh*DF** exhibits a smaller J_{SC}. The AFM results revealed that the addition of the DIO additive enabled the formation of interpenetrating and interconnected phase separation morphology of **P-*h*F** : $PC_{71}BM$ and **P-*h*DF** : $PC_{71}BM$, however, just the reverse for the **P-*eh*DF** : $PC_{71}BM$ case, which were consistent with the photovoltaic performance of these polymers (Table 2).[8,46,49,50]

Conclusions

Three low band gap polymers based on DTS and BT derivatives with different number of F atoms and side chains were designed and synthesized. All the polymers, **P-*h*F**, **P-*h*DF** and **P-*eh*DF**, exhibited excellent solubility and good thermal stability until decomposition temperatures around 420 °C. **P-*h*F**, **P-*h*DF** and **P-*eh*DF** showed narrow E_g^{opt} of 1.56, 1.56 and 1.60 eV with deep lying HOMO energy levels of −5.17, −5.21 and −5.35 eV, respectively. The photovoltaic properties of the polymers were carefully optimized with different polymer/$PC_{71}BM$ weight ratios and additive volume ratios. For the optimized blend of **P-*h*F**, a V_{OC} of 0.553 V, a J_{SC} of 15.51 mA cm^{-2} and a FF of 58.8% were obtained, resulting in a PCE of 5.04%. Contributed by the slightly deeper HOMO energy level and better coplanarity structure, the optimized **P-*h*DF**-based device exhibited higher V_{OC} of 0.593 V, J_{SC} of 15.98 mA cm^{-2}, FF of 64.8% and a higher PCE of 6.14%. The HOMO level of **P-*eh*DF** was 0.14 eV lower than that of **P-*h*DF** due to the bigger dihedral angle between DTS and thiophene which was caused by the increased steric hindrance of 2-ethylhexyl, resulting in a higher V_{OC} of 0.805 V. This was one of the highest V_{OC} values obtained in devices based on polymers with DTS as the electron-rich unit and BT derivatives as the electron-deficient unit. However, the J_{SC} was decreased to 8.01 mA cm^{-2}, which was ascribed to unfavorable surface morphology and low hole mobility caused by the twisted backbone. As a result, the **P-*eh*DF**-based device only gave a PCE of 4.03%. Our work shows that the photovoltaic performance of a polymer can be tuned by the electron withdrawing groups and steric hindrance of side chains.

Experimental

Measurements

^1H NMR spectra were recorded on a Bruker Advance III 600 (600 MHz). UV-vis absorption spectra were recorded at room temperature using a Hitachi U-4100 spectrophotometer. CV measurements were performed on a CHI 660D electrochemical

workstation equipped with a three-electrode cell consisting of a platinum disk working electrode (2.0 mm in diameter), a saturated calomel reference electrode (SCE) and a platinum wire counter electrode. The measurements were carried out in anhydrous acetonitrile containing 0.1 mol L^{-1} tetrabutylammonium phosphorus hexafluoride (Bu_4NPF_6) as the supporting electrolyte under a nitrogen atmosphere at a scan rate of 50 mV s^{-1}. Thin films were deposited from chloroform solution onto the platinum working electrodes and dried under nitrogen prior to measurement. The redox potential of the ferrocene/ferrocenium (Fc/Fc^+) internal reference is 0.39 V *vs.* SCE. HOMO and LUMO energy levels were determined by calculating the empirical formula of HOMO = $-(E_{on}^{ox} + 4.80 - E_{1/2,(Fc/Fc^+)})$, LUMO = $-(E_{on}^{red} + 4.80 - E_{1/2,(Fc/Fc^+)})$, where E_{on}^{ox} is the onset oxidation potential and E_{on}^{red} is the onset reduction potential. TGA and DSC measurements were performed by an STA-409 at a heating rate of 10 °C min^{-1}, under the protection of a nitrogen atmosphere. XRD spectra were recorded on a Bruker D8 Advance. GPC analysis was made using THF as the eluent. The surface roughness and morphology of thin films were characterized by AFM on an Agilent 5400.

Fabrication of polymer photovoltaic devices

Photovoltaic devices were fabricated on 15 mm × 15 mm patterned indium tin oxide (ITO) coated glass substrates with a layered structure of ITO/PEDOT:PSS (40 nm)/polymer:$PC_{71}BM$ blend (~110 nm)/Ca (10 nm)/Al (100 nm). The ITO coated glass substrates were cleaned in ultrasonic bath in acetone, methanol and isopropyl alcohol sequentially. The substrates were treated with oxygen plasma for 6 min, then spin-coated with PEDOT:PSS at 4000 rpm, and annealed in an oven for 20 min at 160 °C. The polymer and $PC_{71}BM$ were dissolved in deoxygenated anhydrous DCB in different weight ratios and the total concentration of the polymer/$PC_{71}BM$ blending solution was 24 mg mL^{-1}. The solutions were stirred overnight in a nitrogen filled glovebox. An active layer consisting of the blend of polymer and $PC_{71}BM$ was then spin-coated on PEDOT:PSS. Subsequently Ca (10 nm) and Al (100 nm) were thermally evaporated under a vacuum of ~2×10^{-4} Pa on top of the active layer as a cathode. The device area was 0.1 cm^2 defined by shadow mask. Photovoltaic performance was characterized under illumination with an AM 1.5G (100 mW cm^{-2}), and *J–V* curves were recorded by using a Keithley 2420. EQE of solar cells was analyzed by a certified Newport incident photon conversion efficiency (IPCE) measurement system.

Materials

All reagents and starting materials were purchased from commercial sources and used without further purification unless otherwise mentioned. All air and water sensitive reactions were performed under a nitrogen atmosphere. THF and toluene were distilled from sodium, with benzophenone as an indicator. 4,4′-Bis(2-ethylhexyl)-5,5′-bis(trimethylstannanyl)-dithieno[3,2-*b*:2′,3′-*d*]silole (DTS-Sn),[25] 4,7-bis(5-bromo-4-hexylthienyl)-5-fluoro-2,1,3-benzothiadiazole (*h*DTFBT-Br),[24] 4,7-bis-(5-bromo-4-hexylthienyl)-5,6-difluoro-2,1,3-benzothiadiazole (*h*DTDFBT-Br)[32] and 4,7-bis(5-bromo-4-(2-ethylhexyl)-thienyl)-5,6-difluoro-2,1,3-benzothiadiazole (*eh*DTDFBT-Br)[32,51] were synthesized according to the previously reported methods.

General synthetic procedure of polymers

The polymers were prepared by the same procedure through the Stille coupling reaction. In a 25 mL round-bottom flask, DTS-Sn (0.19 mmole), *h*DTFBT-Br (*h*DTDFBT-Br or *eh*DTDFBT-Br) (0.19 mmole), tris(dibenzylideneacetone)dipalladium (6 mg) and tris(*o*-tolyl)phosphine (14 mg) were subjected to three cycles of evacuation/nitrogen purging and then 5 mL of anhydrous toluene was added. The oil bath was heated to 110 °C slowly, and the reactant was stirred for 48 h at this temperature under a nitrogen atmosphere. The reaction mixture was cooled down to room temperature and precipitated in 150 mL of methanol. The precipitate was filtered then purified by Soxhlet extraction with methanol, hexane, and $CHCl_3$ in succession. $CHCl_3$ fractions were collected, concentrated, reprecipitated in methanol, and dried under vacuum overnight to give the target polymers.

P-*h*F: DTS-Sn (144.1 mg, 0.194 mmol) and *h*DTFBT-Br (124.7 mg, 0.194 mmol) were used in this polymerization following the above procedure, and the polymer was obtained as a blue solid (143.4 mg, yield 82.2%). ^{1}H NMR (600 MHz, $CDCl_3$): δ (ppm) 8.12 (br, 1H), 7.98 (br, 1H), 7.71 (br, 1H), 7.22 (br, 2H), 2.87 (br, 4H), 1.76 (br, 4H), 1.53–1.16 (br, 34H), 0.98–0.82 (br, 18H). Molecular weight: M_n = 15 400 g mol^{-1}, PDI = 1.86.

P-*h*DF: DTS-Sn (145.4 mg, 0.195 mmol) and *h*DTDFBT-Br (129.4 mg, 0.195 mmol) were used, and the polymer was obtained as a dark blue solid (150.0 mg, yield 83.5%). ^{1}H NMR (600 MHz, $CDCl_3$): δ (ppm) 8.10 (br, 2H), 7.20 (br, 2H), 2.88 (br, 4H), 1.76 (br, 4H), 1.50–1.14 (br, 34H), 1.00–0.80 (br, 18H). Molecular weight: M_n = 16 200 g mol^{-1}, PDI = 1.74.

P-*eh*DF: DTS-Sn (142.0 mg, 0.191 mmol) and *eh*DTDFBT-Br (137.1 mg, 0.191 mmol) were used, and the polymer was obtained as a dark blue solid (133.1 mg, yield 76.2%). ^{1}H NMR (600 MHz, $CDCl_3$): δ (ppm) 8.10 (br, 2H), 7.20 (br, 2H), 2.84 (br, 4H), 1.80 (br, 2H), 1.51 (br, 2H), 1.41–1.20 (br, 36H), 0.93–0.83 (br, 24H). Molecular weight: M_n = 12 800 g mol^{-1}, PDI = 2.19.

Acknowledgements

This work was supported by the National Natural Science Foundation of China (21202181, 21274161, 51173199, and 61107090), Ministry of Science and Technology of China (2014CB643501, 2010DFA52310), and the Department of Science and Technology of Shandong Province (ZR2012BQ021).

Notes and references

1 Y.-J. Cheng, S.-H. Yang and C.-S. Hsu, *Chem. Rev.*, 2009, **109**, 5868–5923.

2 L. Dou, J. You, Z. Hong, Z. Xu, G. Li, R. A. Street and Y. Yang, *Adv. Mater.*, 2013, **25**, 6642–6671.
3 L. Ye, S. Zhang, L. Huo, M. Zhang and J. Hou, *Acc. Chem. Res.*, 2014, **47**, 1595–1603.
4 Z. He, C. Zhong, X. Huang, W. Y. Wong, H. Wu, L. Chen, S. Su and Y. Cao, *Adv. Mater.*, 2011, **23**, 4636–4643.
5 L. Han, W. Chen, T. Hu, J. Ren, M. Qiu, Y. Zhou, D. Zhu, N. Wang, M. Sun and R. Yang, *ACS Macro Lett.*, 2015, **4**, 361–366.
6 H. Lv, X. Zhao, Z. Li, D. Yang, Z. Wang and X. Yang, *Polym. Chem.*, 2014, **5**, 6279–6286.
7 L. Han, X. Bao, T. Hu, Z. Du, W. Chen, D. Zhu, Q. Liu, M. Sun and R. Yang, *Macromol. Rapid Commun.*, 2014, **35**, 1153–1157.
8 H.-C. Liao, C.-C. Ho, C.-Y. Chang, M.-H. Jao, S. B. Darling and W.-F. Su, *Mater. Today*, 2013, **16**, 326–336.
9 J. Wang, M. Xiao, W. Chen, M. Qiu, Z. Du, W. Zhu, S. Wen, N. Wang and R. Yang, *Macromolecules*, 2014, **47**, 7823–7830.
10 C. M. Amb, S. Chen, K. R. Graham, J. Subbiah, C. E. Small, F. So and J. R. Reynolds, *J. Am. Chem. Soc.*, 2011, **133**, 10062–10065.
11 G. Li, R. Zhu and Y. Yang, *Nat. Photonics*, 2012, **6**, 153–161.
12 J. You, L. Dou, K. Yoshimura, T. Kato, K. Ohya, T. Moriarty, K. Emery, C. C. Chen, J. Gao, G. Li and Y. Yang, *Nat. Commun.*, 2013, **4**, 1446.
13 C. C. Chen, W. H. Chang, K. Yoshimura, K. Ohya, J. You, J. Gao, Z. Hong and Y. Yang, *Adv. Mater.*, 2014, **26**, 5670–5677.
14 Y. Liu, J. Zhao, Z. Li, C. Mu, W. Ma, H. Hu, K. Jiang, H. Lin, H. Ade and H. Yan, *Nat. Commun.*, 2014, **5**, 5293.
15 L. Huo, X. Guo, S. Zhang, Y. Li and J. Hou, *Macromolecules*, 2011, **44**, 4035–4037.
16 J.-S. Wu, S.-W. Cheng, Y.-J. Cheng and C.-S. Hsu, *Chem. Soc. Rev.*, 2015, **44**, 1113–1154.
17 J. Peet, J. Y. Kim, N. E. Coates, W. L. Ma, D. Moses, A. J. Heeger and G. C. Bazan, *Nat. Mater.*, 2007, **6**, 497–500.
18 Y. Zhang, J. Zou, C.-C. Cheuh, H.-L. Yip and A. K. Y. Jen, *Macromolecules*, 2012, **45**, 5427–5435.
19 C.-Y. Chang, L. Zuo, H.-L. Yip, Y. Li, C.-Z. Li, C.-S. Hsu, Y.-J. Cheng, H. Chen and A. K. Y. Jen, *Adv. Funct. Mater.*, 2013, **23**, 5084–5090.
20 S. Albrecht, S. Janietz, W. Schindler, J. Frisch, J. Kurpiers, J. Kniepert, S. Inal, P. Pingel, K. Fostiropoulos, N. Koch and D. Neher, *J. Am. Chem. Soc.*, 2012, **134**, 14932–14944.
21 Y. Li, J. Zou, H.-L. Yip, C.-Z. Li, Y. Zhang, C.-C. Chueh, J. Intemann, Y. Xu, P.-W. Liang, Y. Chen and A. K. Y. Jen, *Macromolecules*, 2013, **46**, 5497–5503.
22 C.-Y. Chang, L. Zuo, H.-L. Yip, C.-Z. Li, Y. Li, C.-S. Hsu, Y.-J. Cheng, H. Chen and A. K. Y. Jen, *Adv. Energy Mater.*, 2014, **4**, 1301645.
23 J. Min, Z.-G. Zhang, S. Zhang and Y. Li, *Chem. Mater.*, 2012, **24**, 3247–3254.
24 C. Gu, M. Xiao, X. Bao, L. Han, D. Zhu, N. Wang, S. Wen, W. Zhu and R. Yang, *Polym. Chem.*, 2014, **5**, 6551–6557.
25 J. Hou, H.-Y. Chen, S. Zhang, G. Li and Y. Yang, *J. Am. Chem. Soc.*, 2008, **130**, 16144–16145.
26 T. Y. Chu, J. Lu, S. Beaupre, Y. Zhang, J. R. Pouliot, S. Wakim, J. Zhou, M. Leclerc, Z. Li, J. Ding and Y. Tao, *J. Am. Chem. Soc.*, 2011, **133**, 4250–4253.
27 M. C. Scharber, M. Koppe, J. Gao, F. Cordella, M. A. Loi, P. Denk, M. Morana, H. J. Egelhaaf, K. Forberich, G. Dennler, R. Gaudiana, D. Waller, Z. Zhu, X. Shi and C. J. Brabec, *Adv. Mater.*, 2010, **22**, 367–370.
28 H. Y. Chen, J. Hou, A. E. Hayden, H. Yang, K. N. Houk and Y. Yang, *Adv. Mater.*, 2010, **22**, 371–375.
29 J.-S. Wu, Y.-J. Cheng, T.-Y. Lin, C.-Y. Chang, P.-I. Shih and C.-S. Hsu, *Adv. Funct. Mater.*, 2012, **22**, 1711–1722.
30 C. P. Chen and H. L. Hsu, *Macromol. Rapid Commun.*, 2013, **34**, 1623–1628.
31 S. Ko, E. T. Hoke, L. Pandey, S. Hong, R. Mondal, C. Risko, Y. Yi, R. Noriega, M. D. McGehee, J. L. Bredas, A. Salleo and Z. Bao, *J. Am. Chem. Soc.*, 2012, **134**, 5222–5232.
32 N. Wang, Z. Chen, W. Wei and Z. Jiang, *J. Am. Chem. Soc.*, 2013, **135**, 17060–17068.
33 C.-H. Chen, C.-H. Hsieh, M. Dubosc, Y.-J. Cheng and C.-S. Hsu, *Macromolecules*, 2010, **43**, 697–708.
34 M. J. Frisch, G. W. Trucks, H. B. Schlegel, G. E. Scuseria, M. A. Robb, J. R. Cheeseman, G. Scalmani, V. Barone, B. Mennucci, G. A. Petersson, H. Nakatsuji, M. Caricato, X. Li, H. P. Hratchian, A. F. Izmaylov, J. Bloino, G. Zheng, J. L. Sonnenberg, M. Hada, M. Ehara, K. Toyota, R. Fukuda, J. Hasegawa, M. Ishida, T. Nakajima, Y. Honda, O. Kitao, H. Nakai, T. Vreven, J. A. Montgomery, J. E. Peralta, F. Ogliaro, M. Bearpark, J. J. Heyd, E. Brothers, K. N. Kudin, V. N. Staroverov, R. Kobayashi, J. Normand, K. Raghavachari, A. Rendell, J. C. Burant, S. S. Iyengar, J. Tomasi, M. Cossi, N. Rega, J. M. Millam, M. Klene, J. E. Knox, J. B. Cross, V. Bakken, C. Adamo, J. Jaramillo, R. Gomperts, R. E. Stratmann, O. Yazyev, A. J. Austin, R. Cammi, C. Pomelli, J. W. Ochterski, R. L. Martin, K. Morokuma, V. G. Zakrzewski, G. A. Voth, P. Salvador, J. J. Dannenberg, S. Dapprich, A. D. Daniels, Ö. Farkas, J. B. Foresman, J. V. Ortiz, J. Cioslowski and D. J. Fox, *Gaussian 09, Revision A.1*, Gaussian, Inc., Wallingford, CT, 2009.
35 T. L. Nguyen, H. Choi, S.-J. Ko, M. A. Uddin, B. Walker, S. Yum, J.-E. Jeong, M. H. Yun, T. J. Shin, S. Hwang, J. Y. Kim and H. Y. Woo, *Energy Environ. Sci.*, 2014, **7**, 3040–3051.
36 B. C. Schroeder, Z. Huang, R. S. Ashraf, J. Smith, P. D'Angelo, S. E. Watkins, T. D. Anthopoulos, J. R. Durrant and I. McCulloch, *Adv. Funct. Mater.*, 2012, **22**, 1663–1670.
37 S. Zhang, L. Ye, Q. Wang, Z. Li, X. Guo, L. Huo, H. Fan and J. Hou, *J. Phys. Chem. C*, 2013, **117**, 9550–9557.
38 L. Dou, C.-C. Chen, K. Yoshimura, K. Ohya, W.-H. Chang, J. Gao, Y. Liu, E. Richard and Y. Yang, *Macromolecules*, 2013, **46**, 3384–3390.
39 C. Cabanetos, A. El Labban, J. A. Bartelt, J. D. Douglas, W. R. Mateker, J. M. Frechet, M. D. McGehee and P. M. Beaujuge, *J. Am. Chem. Soc.*, 2013, **135**, 4656–4659.

40 X. Wang, Y. Sun, S. Chen, X. Guo, M. Zhang, X. Li, Y. Li and H. Wang, *Macromolecules*, 2012, **45**, 1208–1216.
41 Z. G. Zhang, J. Min, S. Zhang, J. Zhang, M. Zhang and Y. Li, *Chem. Commun.*, 2011, **47**, 9474–9476.
42 S. C. Price, A. C. Stuart, L. Yang, H. Zhou and W. You, *J. Am. Chem. Soc.*, 2011, **133**, 4625–4631.
43 H.-Y. Chen, J. Hou, S. Zhang, Y. Liang, G. Yang, Y. Yang, L. Yu, Y. Wu and G. Li, *Nat. Photonics*, 2009, **3**, 649–653.
44 L. J. A. Koster, V. D. Mihailetchi and P. W. M. Blom, *Appl. Phys. Lett.*, 2006, **88**, 093511.
45 M. Zhang, X. Guo, W. Ma, S. Zhang, L. Huo, H. Ade and J. Hou, *Adv. Mater.*, 2014, **26**, 2089–2095.
46 H.-C. Chen, Y.-H. Chen, C.-C. Liu, Y.-C. Chien, S.-W. Chou and P.-T. Chou, *Chem. Mater.*, 2012, **24**, 4766–4772.
47 S. Liu, X. Bao, W. Li, K. Wu, G. Xie, R. Yang and C. Yang, *Macromolecules*, 2015, **48**, 2948–2957.
48 G. Ren, E. Ahmed and S. A. Jenekhe, *Adv. Energy Mater.*, 2011, **1**, 946–953.
49 J. M. Lobez, T. L. Andrew, V. Bulović and T. M. Swager, *ACS Nano*, 2012, **6**, 3044–3056.
50 X. Hu, C. Yi, M. Wang, C.-H. Hsu, S. Liu, K. Zhang, C. Zhong, F. Huang, X. Gong and Y. Cao, *Adv. Energy Mater.*, 2014, **4**, 14000378.
51 H. Zhou, L. Yang, A. C. Stuart, S. C. Price, S. Liu and W. You, *Angew. Chem. Int. Ed.*, 2011, **50**, 2995–2998.